

Saturation and response dependence of OSLDs and microStar reader in the high dose range for INTRABEAM kV X-rays and initial investigation into the use of Gafchromic film as an *in vivo* dosimeter in the high dose region

By

Travis Bryant

A THESIS

Submitted to the

Oregon Health & Science University School of Medicine

&

Department of Medical Physics

in partial fulfillment of  
the requirements for the  
degree of

Master of Science

June 2017

School of Medicine  
Oregon Health & Science University

CERTIFICATE OF APPROVAL

This is to certify that the Master's thesis of  
Travis Bryant  
has been approved

---

Mentor/Advisor

---

Member

---

Member

## TABLE OF CONTENTS

	<u>Page</u>
1 INTRODUCTION.....	1
2 MATERIALS.....	2
2.1 INTRABEAM.....	2
2.1.1 INTRABEAM IN THE CLINIC.....	8
2.2 OSLDs.....	10
2.3 MICROSTAR.....	14
2.4 GAFCHROMIC FILM.....	17
3 METHODS.....	17
4 RESULTS.....	22
5 DISCUSSION.....	37
5.1 CLINICAL IMPLICATIONS.....	41
6 CONCLUSIONS.....	42

## LIST OF FIGURES

<u>Figure</u>	<u>Page</u>
1. INTRABEAM device.....	3
2. INTRABEAM applicators with dose distributions.....	3
3. X-ray source (XRS) miniaturized linear accelerator .....	4
4. INTRABEAM spherically isotropic dose distribution .....	5
5. Absolute depth dose curves for different spherical applicators .....	6
6. Percent depth dose curves for different spherical applicators .....	7
7. X-ray spectra at different.....	8
8. Landauer NanoDot OSLD.....	11
9. Band structure of Al <sub>2</sub> O <sub>3</sub> :C crystal.....	13
10. Al <sub>2</sub> O <sub>3</sub> :C crystal energy response dependence.....	14
11. MicroStar components.....	15
12. PMT anode current relationship with incident light intensity.....	16
13. OSLD experimental setup.....	19
14. Gafchromic film experimental setup.....	21
15. MicroStar calibration curve for 2.5 cm applicator.....	23
16. MicroStar calibration curve for 3.0 cm applicator.....	24
17. MicroStar calibration curve for 3.5 cm applicator.....	24
18. MicroStar calibration curve for 4.0 cm applicator.....	25
19. MicroStar calibration curve for 4.5 cm applicator.....	25
20. OSLD saturation curve for 6 MV linac X-rays.....	27
21. OSLD saturation curve for 50 kVp X-rays.....	28

22. OSLD response curve for 2.5 cm applicator.....	30
23. OSLD response curve for 3.0 cm applicator.....	30
24. OSLD response curve for 3.5 cm applicator.....	31
25. OSLD response curve for 4.0 cm applicator.....	31
26. OSLD response curve for 4.5 cm applicator.....	32
27. Gafchromic film calibration curve.....	33
28. Gafchromic film response curve for 2.5 cm applicator.....	36
29. Gafchromic film response curve for 3.0 cm applicator.....	36
30. Gafchromic film response curve for 3.5 cm applicator.....	37
31. Gafchromic film response curve for 4.0 cm applicator.....	37
32. Gafchromic film response curve for 4.5 cm applicator.....	38

## LIST OF TABLES

<u>Table</u>	<u>Page</u>
1. Applicators with corresponding dose rate and treatment times.....	10
2. OSLD calibration curve coefficients of variation.....	25
3. OSLD calibration curve spot checks.....	26
4. OSLD response ratio.....	28
5. OSLD dose rate response.....	29
6. Gafchromic film percent difference of measured vs. expected dose.....	33
7. Gafchromic film dose rate response .....	35

## ACKNOWLEDGEMENTS

I would first and foremost like to thank my advisor Susha Pillai. I can say with full conviction that without her constant guidance and patience I would not have been able to complete my research and thesis. I would like to thank Dr. Krystina Tack who taught me the foundations of medical physics, and has shown me great compassion and understanding throughout my time at OHSU. I would like to thank Dr. Richard Crilly for always taking the time to answer my questions. I would also like to thank my fellow students, without whom my graduate studies would have been much more difficult.

## ABSTRACT

### BACKGROUND

Oregon Health and Science University (OHSU) performs intraoperative radiotherapy (IORT) in conjunction with Breast-conserving surgery (BCS) for early stage breast cancer. IORT procedures are performed using the Carl Zeiss INTRABEAM device which uses a miniature X-ray probe with spherical applicators and delivers dose to the lumpectomy bed using low kV superficial X-rays of 50 kVp. Landauer® NanoDot Optically Stimulated Luminescence Dosimeters (OSLD) in conjunction with the Landauer® microStar reader were



used to meet the unique low energy *in vivo* dosimetry requirements to measure dose to the skin close to the treatment area. However, the characteristics of OSLDs have not been thoroughly investigated in the dose range of superficial energies. The purpose of this study is to investigate the properties of OSLDs under these conditions and to preliminarily investigate the properties and potential usage of gafchromic EBT 3 film for INTRABEAM *in vivo* dosimetry.

## METHODS

The INTRABEAM system utilizes different size spherical applicators to deliver dose based on the resultant size of the lumpectomy cavity. In this experiment a dose of 20 Gy was delivered to the surface of five different spherical applicators with diameters of 2.5, 3.0, 3.5, 4.0, and 4.5 cm. Both OSLDs and gafchromic film were irradiated by each of these applicators in a water medium at different depths of 0.5, 1.0, 1.5, 2.0, and 3.0 cm to investigate dosimeter response to varying energies, dose accumulation, and dose rates. The Landauer® microStar reader was used to read the irradiated OSLDs. The irradiated gafchromic films were scanned in an Epson 10000 XL flatbed scanner and DoseLab software was used to find the mean intensity values at the field center. Calibration and response curves for both OSLDs and EBT3 films were constructed to further study both types of dosimeters.

## RESULTS

The OSLD calibration curves start to become unreliable in the 10 Gy to 15 Gy range due to potentially both nanoDot sensitivity change and microStar reader saturation. Further, there is evidence to indicate that OSLD response is dependent on energy and dose accumulation<sup>1</sup>. Gafchromic film calibration curves show the potential to be used in the high dose range above 10 Gy; however, our experiment was inconclusive in the low dose range.

## CONCLUSION

OSLD dosimetry in the dose range below about 10 Gy is shown to be accurate with acceptable tolerance. Further research is proposed to investigate gafchromic film calibration curves and the dose accumulation and energy dependence of the OSLDs and gafchromic film.

## 1 INTRODUCTION

Oregon Health and Science University (OHSU) performs intraoperative radiotherapy (IORT) in conjunction with Breast-conserving surgery (BCS) for early stage breast cancer. IORT procedures are performed using the Carl Zeiss INTRABEAM device which uses a miniature X-ray probe with spherical applicators and delivers a dose of 20 Gy to the lumpectomy bed using low kV superficial X-rays of 50 kVp. Currently, Landauer® nanoDot Optically Stimulated Luminescence Dosimeters (OSLD) in conjunction with the Landauer® microStar reader are used to meet the unique low energy *in vivo* dosimetry requirements to measure dose to the skin close to the treatment area. However, OSLDs dosimetry has limitations and many of the physical characteristics have not been documented for this particular kV energy range.

OSLD calibration curves are limited to about 10 Gy for INTRABEAM procedures. This is due to signal saturation which is a result of both OSLD sensitivity decline at larger accumulated doses and microStar reader saturation. There is currently no literature investigating the region where this signal saturation occurs for X-rays of this energy range. OSLD response dependence has been shown to be largely independent of energy in the MV range. It is known that in the diagnostic energy range that OSLDs are energy dependent and show an over response. The INTRABEAM's X-ray energy is below the diagnostic range. The effect of the steep spectral shift and OSLD energy dependence on response has not been thoroughly investigated for this energy

range. Further, the effects of dose rate and dose accumulation in this energy range have not been documented.

There is currently no literature available documenting the creation of calibration curves in the 50 kVp energy range for doses above about 10 Gy. The 10 Gy limitation of OSLD dosimetry justifies a preliminary investigation into the possible use of Gafchromic EBT 3 film to meet the dosimetric needs of the IORT procedure up to the desired 20 Gy. In addition, there are very few articles investigated films response dependence on dose rate, dose accumulation, and energy in this unique energy range for high doses.

## 2 MATERIALS

### 2.1 INTRABEAM

The Carl Zeiss INTRABEAM system, shown in figure 1, is a portable IORT device that delivers a 50 kVp isotropic X-ray beam. It utilizes different applicators attached to the X-ray source (XRS) to modify dose delivery for varying procedures. Figure 2 shows the spherical, flat, surface, and needle applicators and their corresponding dose distribution<sup>2</sup>. The spherical applicator is used on brain tumors and in conjunction with breast conserving surgery post lumpectomy. The flat applicator is used for surgically exposed surfaces such as tumors of the gastrointestinal tract. The surface applicator is

used for non-melanoma skin cancers. The needle applicator is used for vertebral metastases and brain tumors.



Figure 1: INTRABEAM device



Figure 2: Respectively from top to bottom, the spherical, flat, surface, and needle applicators and dose distribution.

The X-rays are produced by the XRS miniaturized linear accelerator seen in figure 3<sup>3</sup>. The XRS utilizes a cathode gun to input electrons into the waveguide. Here the electrons are accelerated to a potential of 50 kV toward the beam deflectors. The beam deflector focuses the electrons through the 100mm long and 3 mm wide drift tube onto the 1 mm thick gold target. The gold target is uniquely shaped to create a spherically isotropic dose distribution as seen in figure 4<sup>2</sup>.

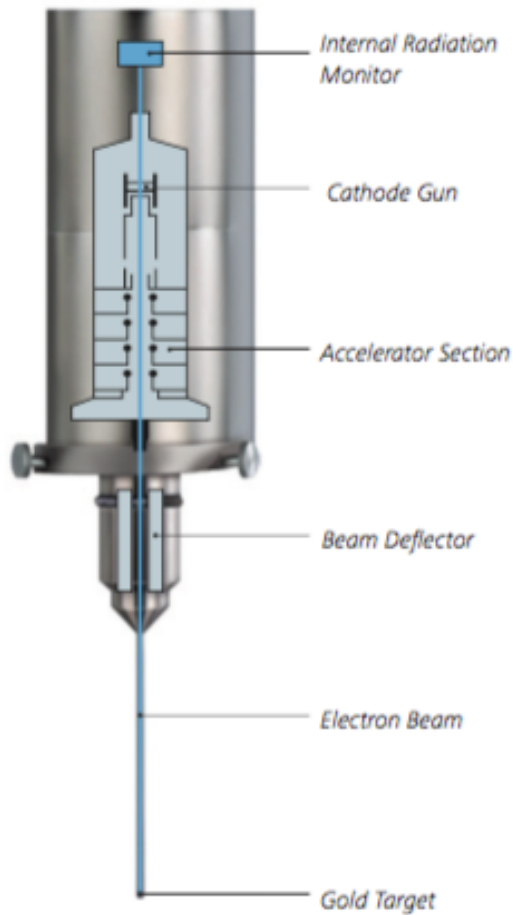


Figure 3: X-ray source (XRS) miniaturized linear accelerator

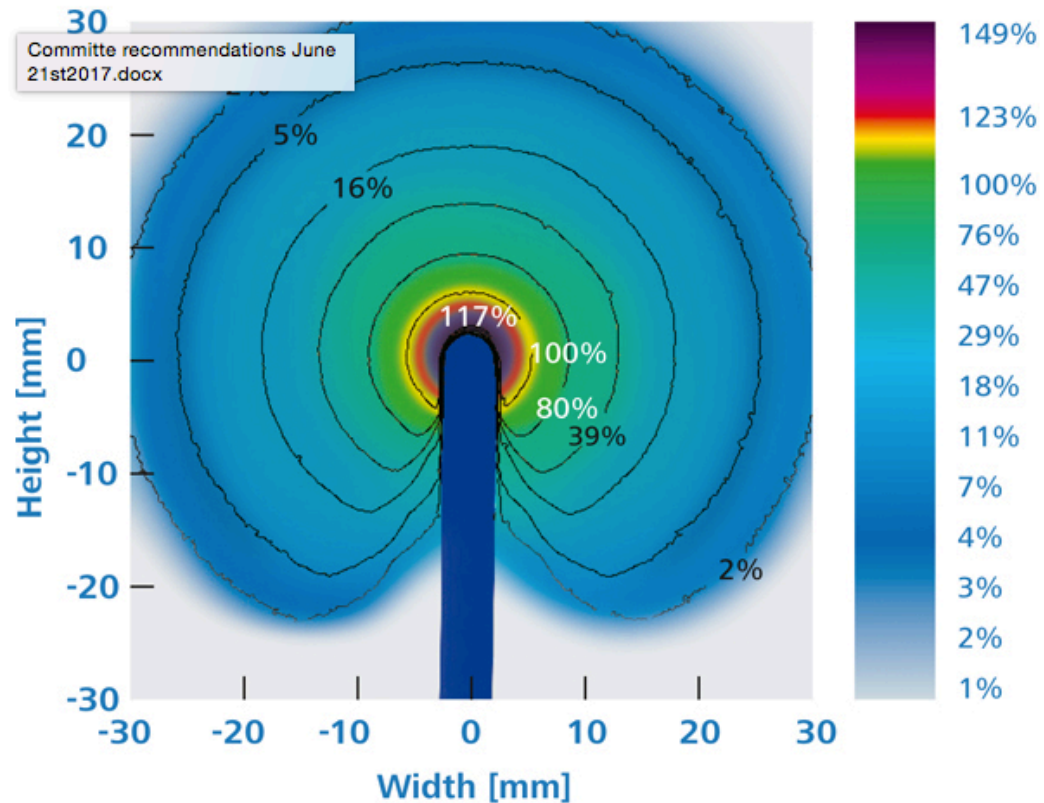


Figure 4: INTRABEAM spherically isotropic dose distribution

The dose distribution and depth dose curves are determined by the manufacturer during production and recalibration. An in depth explanation of this process can be found in the Carl Zeiss provided document, “INTRABEAM Dosimetry”<sup>4</sup>. Essentially, this is accomplished using a soft X-ray ionization chamber contained in a solid water holder that protrudes into a water phantom. This prohibits measurements directly on the surface of the XRS tip. An analytical function is used in this region with the dose being inversely proportional to the depth cubed. The clinically relevant curves used at OHSU for treatment planning are the absolute depth dose curves and the percent depth dose curves with different size spherical applicators shown in Figure 5

and Figure 6, respectively<sup>4,5</sup>. It is observed that the 2.5 and 3.5, and the 3.0 and 4.0 cm spherical applicators dose rate are similar. This is because, even though the surface of the applicator is a different distance from the source of the X-rays, the head of the applicators contains varying amounts of Aluminum that filters the X-rays and modifies the dose rate.

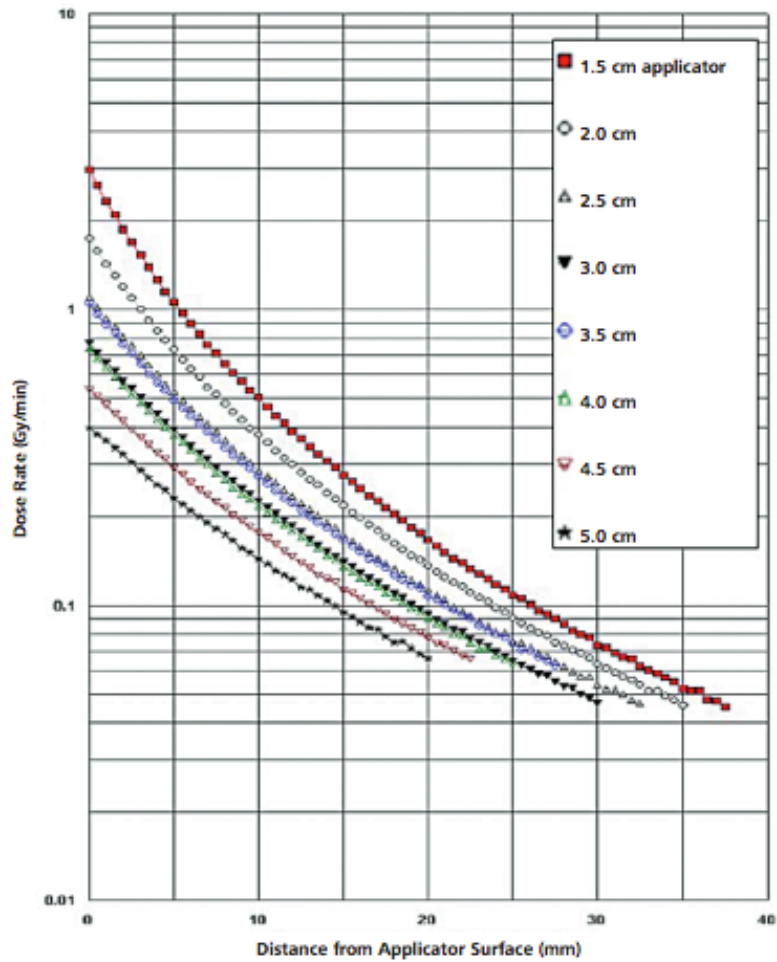


Figure 5: Absolute depth dose curves for different spherical applicators



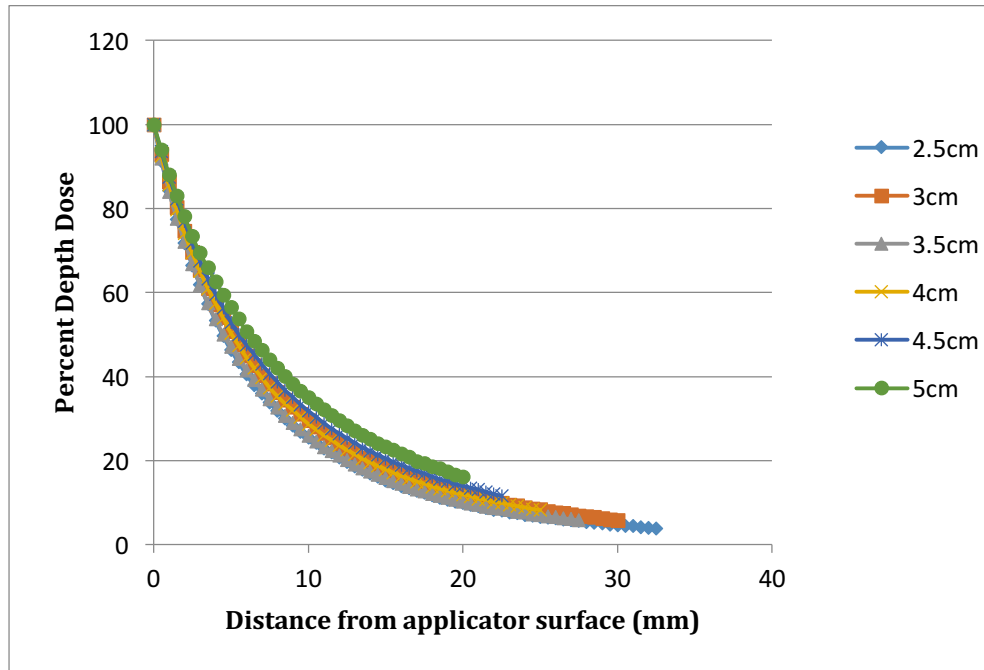


Figure 6: Percent depth dose curves for different spherical applicators

Figure 7 shows the energy spectrum of the bare probe in air and of the probe with the 4.0 cm spherical applicator attached at different depths in a water medium normalized at the 35 keV value<sup>6</sup>. There is an upward spike at about 10 keV for the bare probe that is not seen when the applicator is used. This is due to the aluminum in the head of the applicator. It hardens the beam and filters out the low energy spike. Further, it is observed that the 50 kVp X-rays harden rapidly at depth through the water medium.

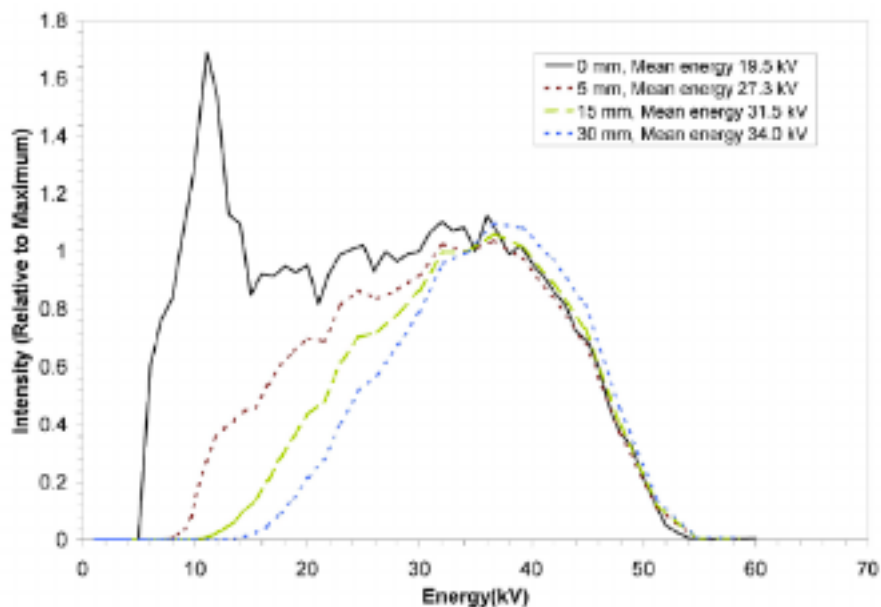


Figure 7: X-ray spectra at different depths in water with 4.0 cm spherical applicator. The 0 mm spectrum is the bare probe in air. All spectra intensity values are normalized at 35 kV.

### 2.1.1 INTRABEAM IN THE CLINIC

The clinical advantage of the INTRABEAM device is that it allows for a highly targeted radiation treatment with greater normal tissue sparing than external beam therapies. The 50 kVp X-rays deliver most of their dose in the first two centimeters of tissue surrounding the tumor cavity due to its steep dose gradient. This low energy offers a higher relative biological effectiveness (RBE) than high energy external radiation due to a higher concentration of ionization. The RBE was calculated for the 4.0 cm spherical applicator with a reference radiation of 6MV, and found to be in the range of 1.26 to 1.42 at 8.1 mm depths<sup>5</sup>. As the depth increases, the RBE decreases and the survival curves suggest little difference between the 50 kVp and 6 MV at 22.9 mm<sup>8</sup>.

OHSU utilizes the INTRABEAM system for BCS in early stage breast cancer post lumpectomy. The prescribed dose at the surface of all the applicators is 20 Gy for this procedure. The targeted intraoperative radiation therapy (TARGIT) clinical trials highlight the advantages of using the INTRABEAM for BCS versus traditional external beam radiotherapy (EBRT)<sup>8</sup>. There is no significant statistical difference in local recurrence of the tumor after 5 years. The mortality rate due to cardiovascular complications and other cancers shows a statistically significant decrease when using the INTRABEAM. In addition, there is a statistically significant reduction in patients with grade 3 or 4 skin complications with the INTRABEAM. The recurrence rate for patients who receive an INTRABEAM boost is about a half to a third of those who received only traditional EBRT. Further, there are advantages to the patient. A traditional EBRT procedure is delivered in fractions split over about 6 weeks. With an INTRABEAM procedure the patient receives one fraction that lasts about 20 to 50 minutes. Table 1 shows the time of an INTRABEAM procedure to deliver 20 Gy to the surface of each of the applicators. This reduction in treatment time minimizes the patient burden and psychological stress. Patients also report better cosmetic results with the INTRABEAM procedure<sup>9</sup>. Lastly, patients ineligible for traditional EBRT in many cases can still receive therapy with the INTRABEAM system<sup>3</sup>.

Applicator Diameter (cm)	Dose Rate (Gy/min)	Treatment Time (min)
2.5	1.165	16.95
3	0.777	25.4
3.5	1.025	19.3
4	0.759	26
4.5	0.55	35.9
5	0.402	49.1

Table 1: Applicators with corresponding dose rate and treatment times

## 2.2 OSLDs

The Landauer manufactured nanoDOT dosimeter, shown in figure 8, is 1 x 1 cm and 0.2 cm thick. Its shell is a light proof plastic case, marked with a serial number that identifies the individual nanoDot. Inside is a 4 mm diameter Aluminum Oxide crystal that has been melted at high temperatures and recrystallized with Carbon added as a dopant<sup>7</sup>. The resultant Al<sub>2</sub>O<sub>3</sub>:C crystal has Oxygen vacancies that create the unique property of Optically Stimulated Luminescence (OSL). Individual crystals will have slightly different molecular structures that creates different dosimetric sensitivities. Sensitivity information is recorded in the barcode of each nanoDOT and comes from either an average from a sampling of the population or individual screening of the nanoDot. This experiment utilizes the individually screened nanoDots that offer a Landauer specified 5% accuracy.



Figure 8: Landauer NanoDot OSLD

Materials with OSL properties have a similar composition and band structure as semiconductors. A semiconductor with a donor dopant increases the electron concentration of the crystal lattice. These additional electrons are negative charge carriers and require a low amount of energy to be excited from the band gap to become free electrons in the conduction band. Semiconductor with an acceptor dopant decreases the electron concentration of the crystal lattice. The electron vacancy is referred to as a hole and is a positive charge carrier. The OSL emission spectrum from this crystal shows that it does not exhibit this simple donor or acceptor type behavior<sup>8</sup>. This is where materials with OSL properties differ from semiconductors, as they contain both positive and negative charge carriers. It is this property that allows for this crystal to be utilized for dosimetry.

Figure 9 taken from Landauer's "The microStar Reader Quality Assurance Program" shows a good representation of the band structure and traps<sup>1</sup>. The following is a summary of the interaction between ionizing radiation and the  $\text{Al}_2\text{O}_3:\text{C}$  crystal. For further information, see Jursinic's paper titled, "Characterization of optically stimulated luminescent dosimeters, OSLDs,

for clinical dosimetric measurements”<sup>10</sup>. When ionizing radiation is incident on the Aluminum Oxide Crystal a charge separation occurs. This causes an electron to move from the valence band to the conduction band and a hole to move to the valence band. This process is represented as A in Figure 3. The electrons can fall from the valence band into one of three electron traps. These electron traps are a superficial, intermediate or dosimetric, and the deep traps represent by C, D, and E in figure 9, respectively. Electrons in the superficial trap are unstable at room temperature with a half-life of 0.5 to 0.9 minutes depending on slight differences in the molecular structures<sup>10</sup>. The electrons in the deep trap can only be released with high temperatures or UV light. The electrons in the intermediate or dosimetric trap can be released by optical stimulation that is provided by the LEDs in the microStar reader. The letter B in figure 9 represents a deep trapping of a hole. This hole can recombine with an electron in the dosimetric trap after optical stimulation as represented by the letter F in Figure 9. The energy of this recombination is emitted as a photon and this is the signal that is used to measure dose.

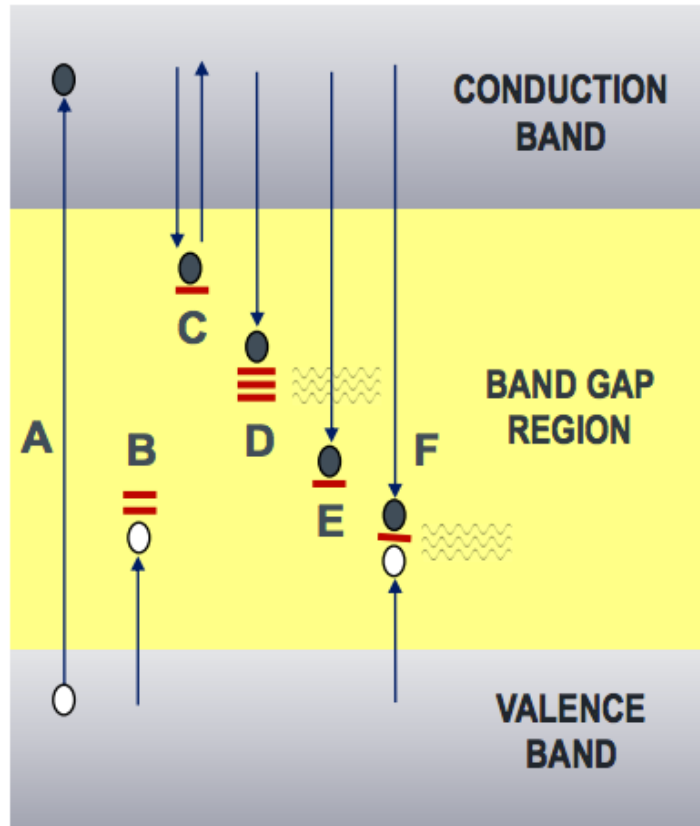


Figure 9: Band structure of  $\text{Al}_2\text{O}_3:\text{C}$  crystal

The photon count data from the electron and hole recombination is proportional to the absorbed dose. Figure 10 shows how the OSLDs response changes with energy<sup>11</sup>. It is observed that in the superficial energy range there is a much greater response than in the MV range. This is due to the increase in mass-energy absorption due to the photoelectric effect at low energies.

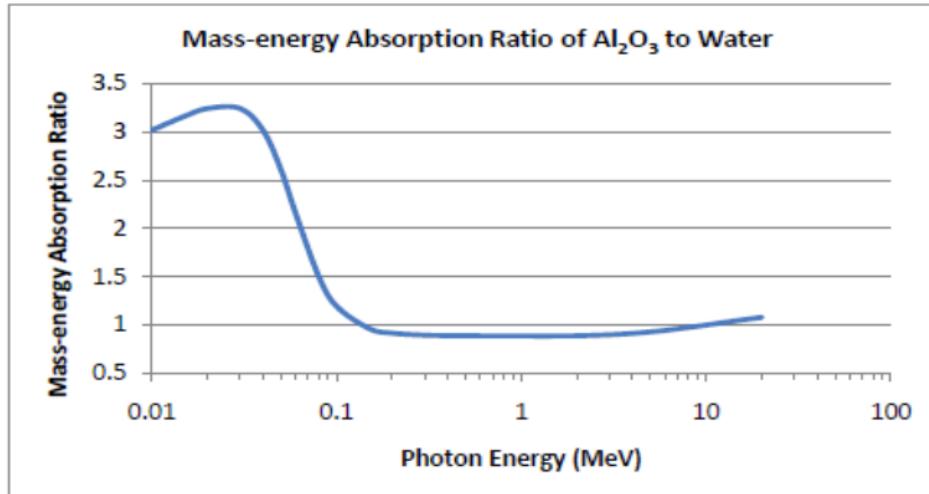


Figure 10: Al<sub>2</sub>O<sub>3</sub>:C crystal energy response dependence

### 2.3 MICROSTAR

OSLDs can be read with either continuous wave optically stimulated luminescence (CW-OSL) or pulsed optically stimulated luminescence (POSL). POSL readers are more accurate because the emission photons are only read between stimulation pulses; however, they are costlier and less portable<sup>12</sup>. The Landauer microStar is a continuous wave optically stimulated luminescence (CW-OSL) reader. Figure 11 is a schematic of the Landauer inlight microStar system<sup>6</sup>.

Jursinic et al provides a good description of the microStars components represented in Figure 11<sup>10</sup>. The microStar generates stimulation light that includes 532 nm wavelength green light utilizing a series of LEDs. The green light then passes through a band-pass filter that minimizes light that isn't 532



nm. This filtered light is then focused on the active  $\text{Al}_2\text{O}_3:\text{C}$  layer inside of the nanoDot OSLD. The electrons trapped in the dosimetric and shallow traps are stimulated into the conduction band before a portion falls into the valence band releasing energy in the form of photons. These emission photons are then passed through a 420 nm band-pass filter. This filter discriminates between emission light and stimulation light, minimizing scattered stimulation light. This weak filtered signal is guided into a photomultiplier tube (PMT) for amplification.

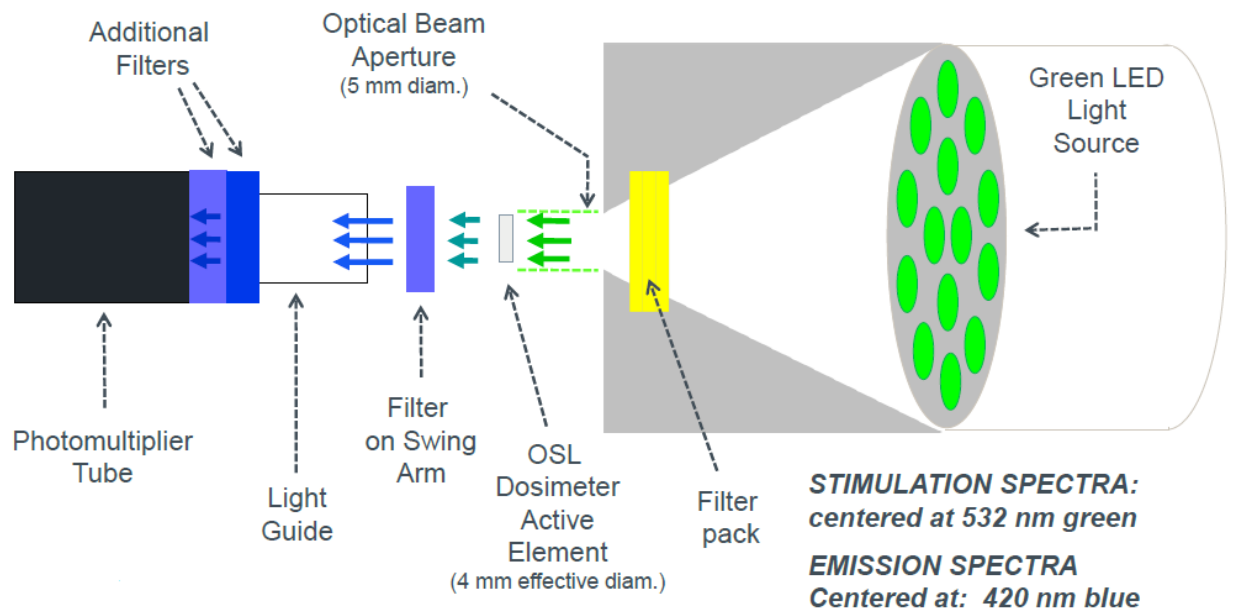


Figure 11: MicroStar components

The 420 nm emission spectra photons incident on a PMT tube will first strike a photocathode. This layer converts the photons into primary electrons. These primary electrons are then focused onto a series of dynodes with a

voltage bias. The dynodes act as electron multipliers by creating electron avalanches. The electrons reach the anode after passing through all of the dynodes and create a current pulse. This pulse is then converted to net charge counts.

Figure 12 shows the relationship between light incident on the PMT and the output anode current<sup>13</sup>. Where the anode current starts to flatten is called the saturation region of the PMT. This occurs because the dynodes have a limit to the number of electrons they can emit at a given voltage bias. This saturation region creates a problem when measuring dose because beyond a certain amount of incident light from the OSLD additional dose will not be counted or will be under counted.

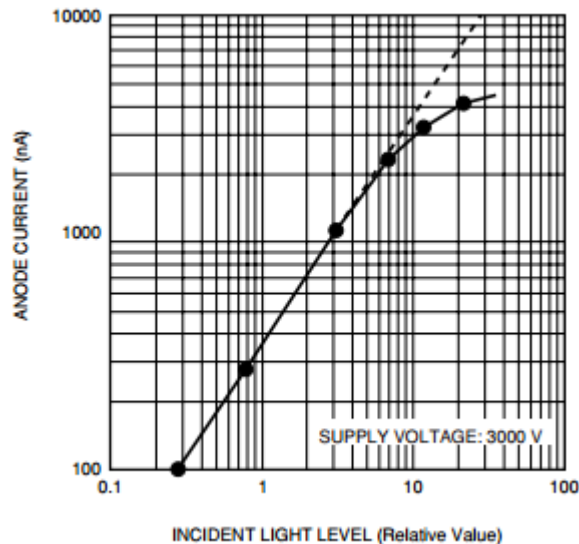


Figure 12: PMT relationship between incident light and anode current

## 2.4 GAFCHROMIC FILM

The characteristics of the Gafchromic EBT 3 film are similar to Gafchromic EBT 2 film except there is no dependence on which side of the film is scanned<sup>14</sup>. The following is a brief summary of Gafchromic EBT 3 film, a more comprehensive overview can be found in the white paper “Gafchromic™ Dosimetry Media, type EBT-3”<sup>15</sup>. The film is near tissue equivalent making it ideal for dosimetry. The film consists of a 28 micrometer thick active layer containing a marker dye and stabilizers. This active layer is sandwiched between two 125 micrometer thick polyester substrates. The film shows a low energy, dose rate, and dose fractionation dependence from the diagnostic to the therapeutic energy ranges and has a dynamic dose range from 0.1 to 20 Gy. The EPSON 10000 XL scanner can read the film in either the red, green, or blue color channel depending on the desired dose range and response characteristics. DoseLab software was used to analyze the film. This software outputs an intensity value which is the optical density multiplied by 17500 to better match the range of 16 bit integers<sup>16</sup>.

## 3 METHODS

This experiment has several goals in the testing of OSLDs and Gafchromic film. First, is a validation of our method of constructed OSLD calibration curves for INTRABEAM *in-vivo* dosimetry for early stage breast cancer for each

applicator. This validation will serve double duty to check for the error in the experimental design. This is done by constructed calibration curves and performing spot checks for each applicator. The next goal of this experiment is to find the dose region where signal saturation occurs in the microStar reader. Lastly, the OSLDs response dependence on dose rate, dose accumulation, and energy will be investigated.

One of the main objectives of this study is to investigate the application of Gafchromic film as an *in-vivo* dosimeter for breast IORT procedures using the INTRABEAM System. Previous efforts have shown a minimal energy dependence in the superficial range<sup>17</sup>. The white paper “Gafchromic™ Dosimetry Media, type EBT-3” claims that the film has a dynamic dose range of 0.1 to 20 Gy indicating no saturation in our desired dose range, and shows minimal dose rate dependence<sup>15</sup>. This will be tested by assuming dose rate, dose accumulation, and energy independence in the construction of the calibration curve. The calibration curve will also be used to investigate film saturation. These properties and films potential application in dosimetry will be further investigated through response curves created at the same depths and doses as the OSLD calibration curves for each applicator.

The OSLD data was collected by taking INTRABEAM measurements in a CNMC Model WP – 3840 water tank at varying distances for each applicator. The OSLDs were first water proofed with a thin layer of cellophane and attached to a mechanical crank accurate to 0.01 cm. The INTRABEAM applicator surface was manually placed above the active crystal in the OSLD. The mechanical

crank was then zeroed and moved to the desired depth as seen in Figure 13. Irradiated OSLDs were then allowed to sit for at least 10 minutes to evacuate the superficial traps before the count data was read by the microStar.

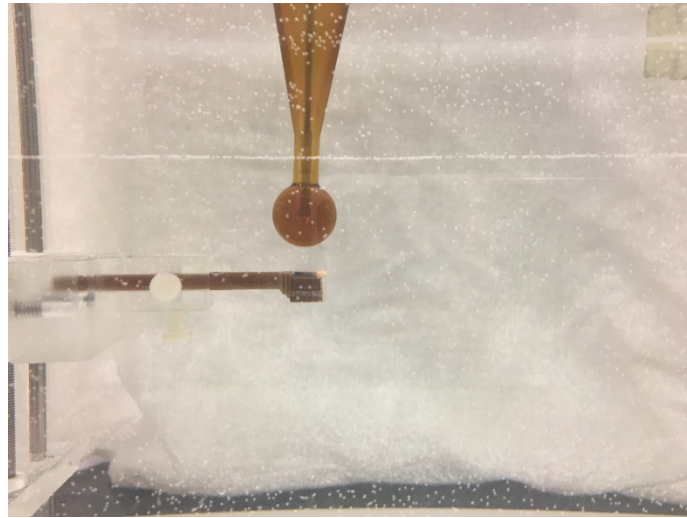


Figure 13: OSLD on mechanical crank moved to desired depth

Previous OSLD calibration curve efforts have shown that each applicator must have its own curve to be accurate<sup>18</sup>. The OSLD calibration curves were created by taking two INTRABEAM measurements in a water tank at varying distances of 0.5, 1.0, 1.5, 2.0 and 3.0 cm for each applicator. The dose delivered was a constant 20 Gy to the surface of the applicator. Distances less than 0.5 cm were not included because it has been shown calibration curves for OSLDs to be inaccurate in this dose range<sup>18</sup>. Further, the experimental design has large errors at this depth. Uncertainty in doses can be greatly affected by uncertainty in dosimeter position due to the steep dose gradient. An uncertainty of 1 mm

causes a dose uncertainty of 45% at the 0.5 cm position<sup>5</sup>. The data used to construct the calibration curves is further used to investigate dose rate dependence and to create response curves to investigate dose accumulation and energy dependence.

Spot checks were performed at three random distances for each applicator. This was done to compare the dose calculated from the calibration curves created as stated in the above paragraph and the known dose output by the INTRABEAM. This allows us to check the accuracy of our calibration curves and experimental design.

OSLDs have an over response in the low energy range. This means that the point of saturation is at a lower dose than for the higher MV energies. The point of saturation for the microStar was investigated by taking measurements in the same method as stated above except the dose was delivered to the 0.5 cm depth in increments of 100, 300, 500, 800, 1000, 1500, and 2000 cGy. The measurements are then compared to measurements taken using a 6 MV linac. These measurements were taken in increments of 10, 100, 300, 500, 800, 1000, 1300, 1500, 2000, 2500, 3000, 5000, 10000 cGy at an SSD of 100 cm at a dmax depth of 1.5 cm in a solid water phantom.

The film data was collected by taking INTRABEAM measurements in a CNMC Model WP – 3840 water tank at varying distances for each applicator. The film was cut into sections of about 2 x 5 inches. The side of these sections were taped to prevent water damage. Each film strip was then placed into a plastic case that held the edges but exposed the center directly to the

INTRABEAM applicators. The strips were then attached to a mechanical gear that could lower the strips to distances accurate to 0.01 cm. The INTRABEAM applicator surface was manually placed above the center of the Gafchromic film as seen in Figure 14. The mechanical crank was then zeroed and moved to the desired depth. The INTRABEAM device was turned on and the film was irradiated. The film was allowed to sit for 72 hours before being scanned. The film was scanned utilizing the green color channel with an Epson 10000 XL flatbed scanner. DoseLab software was then used to find the average intensity value of a 2 x 2 mm square around the field center.

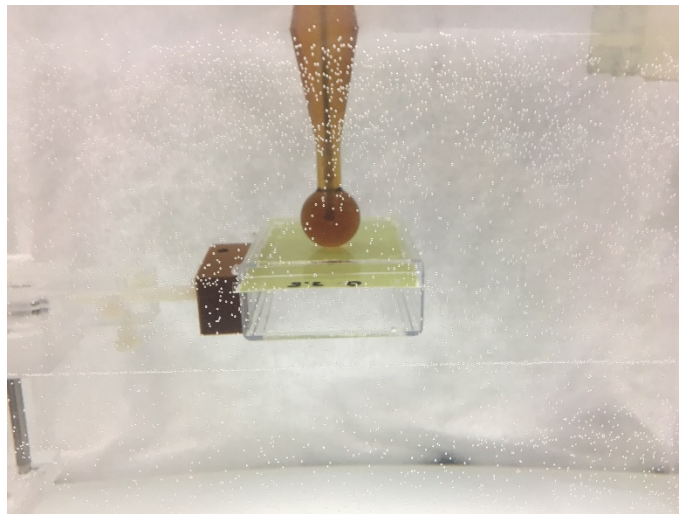


Figure 14: Film on mechanical crank at zeroed position

The calibration curves for the Gafchromic film are assumed independent of dose rate, dose accumulation, and energy. This means that a single calibration curve could potentially be constructed from any of the individual applicators and used for the other applicators. This calibration curve was created by taking INTRABEAM measurements delivered to the 0.5 cm depth in

increments of 100, 300, 500, 800, 1000, 1500, and 2000 cGy for the 3.5 cm applicator. The assumption of dose rate, dose accumulation, and energy independence will be tested by using the calibration curve to calculate dose from film measurements for each applicator at depths of 0.5, 1.0, 1.5, 2.0, and 3.0. This calculated dose is then compared to the known dose output by the INTRABEAM. The percent difference should be low if these assumptions are true. The data used to test the calibration curves is further used to investigate dose rate dependence and to create response curves to investigate dose accumulation and energy dependence.

#### 4 RESULTS

The OSLD count data was recorded after allowing the microStar to warm up for 30 minutes and performing daily microStar QA. The OSLDs were allowed to sit for at least ten minutes before reading to allow for the superficial traps to be evacuated. The Gafchromic film data was collected using an Epson 10000XL flatbed scanner and Dose Lab software. The film was scanned after 72 hours of development time, using 126 dots per inch (dpi), and the green channel in transmission mode. The scanning protocol outlined by Valeria Caxanova Borca et al. was followed to prevent scanning artifacts<sup>14</sup>.

Figures 15 through 19 show the microStar Calibration Curves for the 2.5, 3.0, 3.5, 4.0, and 4.5 cm applicators, respectively. These curves were created by taking two measurements at the depths of 0.5, 1.0, 1.5, 2.0, and 3.0 cm in the



water tank for each applicator. The two OSLDs were then read three times each. The average and standard deviation of these six reading was taken and used to find the coefficient of variation. The coefficient of variation (CV), which gives the relative magnitude of the standard error, was below the tolerance level of 0.05 at each measurement depth for each applicator as shown in Table 2. The calibration curves were closely fitted with third order polynomial trend lines.

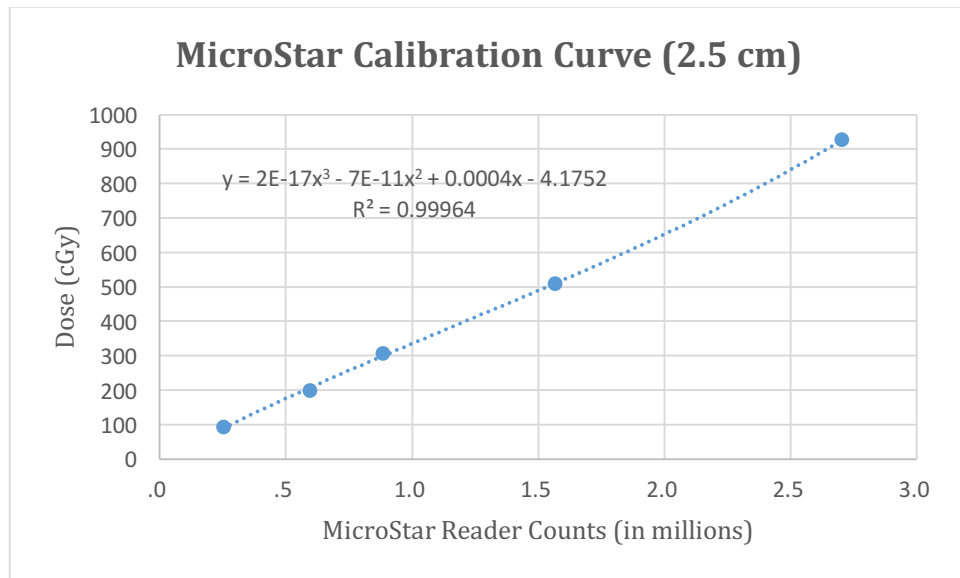


Figure 15: MicroStar calibration curve for the 2.5 cm applicator

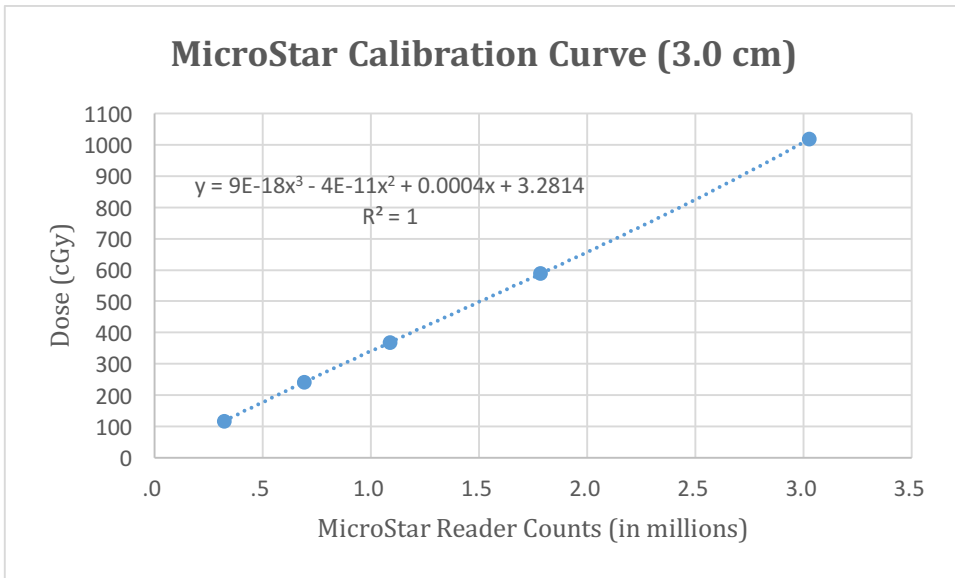


Figure 16: MicroStar calibration curve for the 3.0 cm applicator

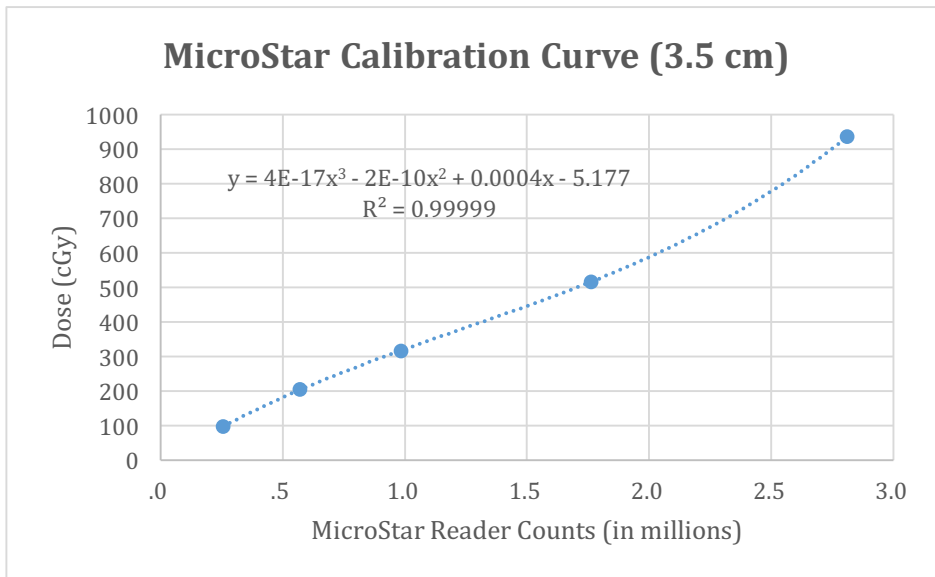


Figure 17: MicroStar calibration curve for the 3.0 cm applicator

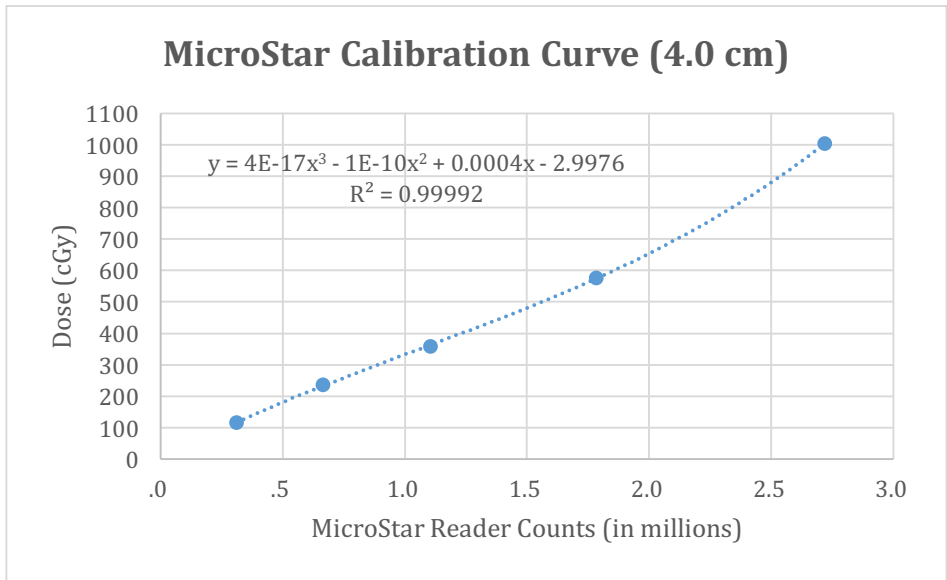


Figure 18: MicroStar calibration curve for the 4.0 cm applicator

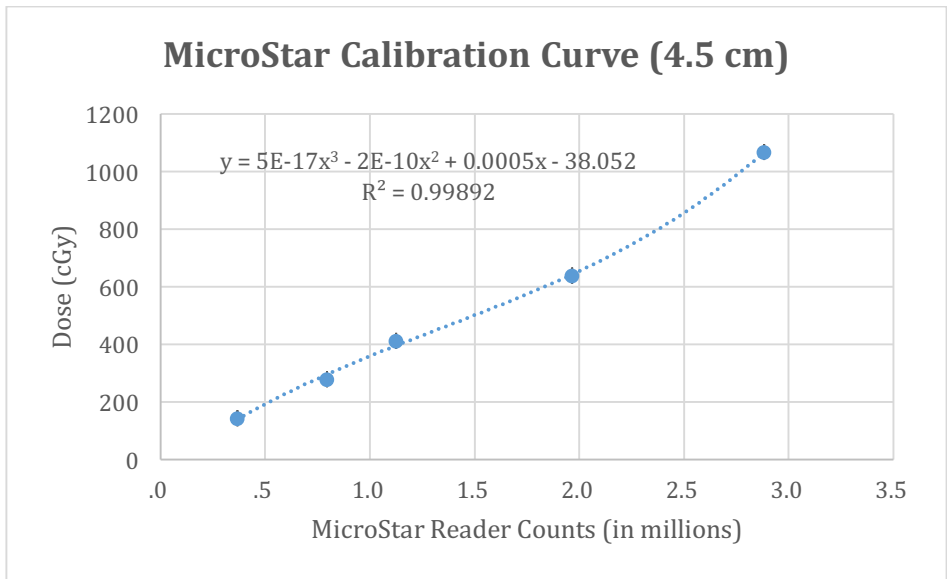


Figure 19: MicroStar calibration curve for the 4.5 cm applicator

Depth (mm)	2.5 cm Diameter Applicator	3.0 cm Diameter Applicator	3.5 cm Diameter Applicator	4.0 cm Diameter Applicator	4.5 cm Diameter Applicator
.5 mm	0.028	0.019	0.009	0.027	0.012
1.0 mm	0.014	0.021	0.007	0.041	0.009
1.5 mm	0.016	0.013	0.012	0.012	0.021
2.0 mm	0.039	0.023	0.008	0.017	0.016

3.0 mm	0.014	0.012	0.009	0.036	0.046
--------	-------	-------	-------	-------	-------

Table 2: Coefficients of variation of the calibration curves for each applicator

Three OSLD spot check measurements were taken for each applicator at randomized depths. Each OSLD spot check was read three times and an average count value was found. The dose was then calculated by plugging the average count value into the appropriate microStar calibration curve equation. These calculated doses were compared to the known dose output by the INTRABEAM device. The percent differences for these spot checks were calculated and tabulated in Table 3. The spot checks showed a high level of agreement given the known uncertainty from experimental set-up, OSLD, and microStar readout.

Applicator Diameter (cm)	Depth (cm)	Expected Dose (cGy)	Calculated Dose (cGy)	Percent Difference
2.5	0.9	568	584.66	2.93
2.5	1.7	256	262.99	2.73
2.5	2.2	168	170.56	1.52
3.0	0.25	1398	1395.11	0.21
3.0	0.8	724	710.93	1.81
3.0	2.3	192	176.74	7.95
3.5	0.7	881	842.85	4.33
3.5	1.2	414	382.49	7.61
3.5	1.8	249	249.87	0.35
4.0	1.3	431	390.42	9.41
4.0	1.6	329	289.19	12.10
4.0	2.5	163	159.71	2.02
4.5	0.8	776	815.47	5.09
4.5	1.4	447	454.90	1.77
4.5	2.7	172	178.22	3.61

Table 3: Spot checks of the microStar calibration curves of each applicator at three different measurement depths showing the percent difference between expected and calculated dose.

Figure 20 shows saturation for a 6 MV linac beam. This curve was created by taking measurements of 10, 100, 300, 500, 800, 1000, 1300, 1500, 2000, 2500, 3000, 5000, 10000 cGy in a solid water phantom. Figure 21 shows saturation for the 50 kVp with the 3.5 cm applicator. This curve was created by taking measurements of 100, 300, 500, 800, 100, 1500, and 2000 cGy at 0.5 mm depth in the water tank. These OSLDs were all read three times each and the average of these values was taken. The saturation effect is seen in the higher dose region for both the 6 MV linac beam and the 3.5 cm applicator where the curve starts to become vertical. It is observed that MV and kV reach saturation at difference doses, but similar count values.

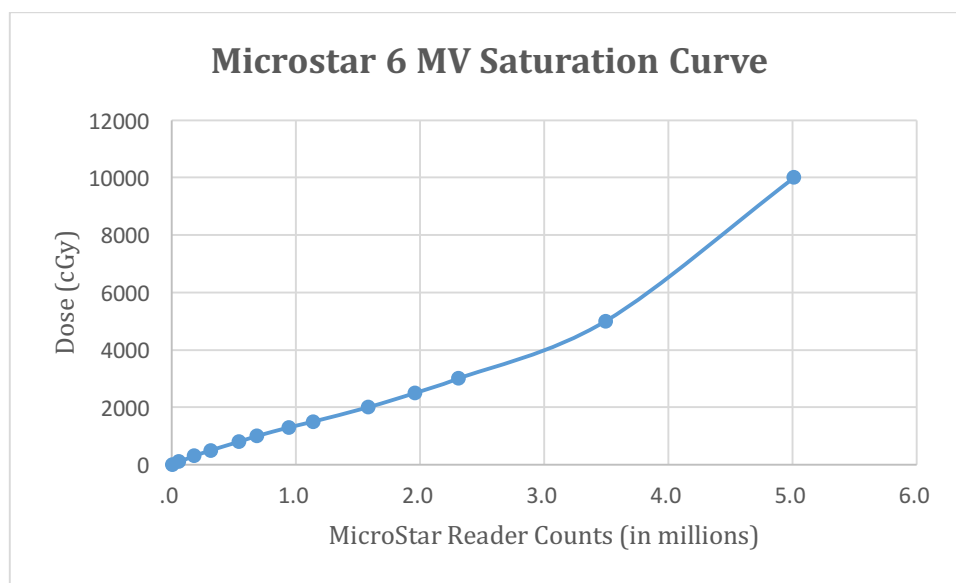


Figure 20: OSLD saturation curve for 6 MV X-ray

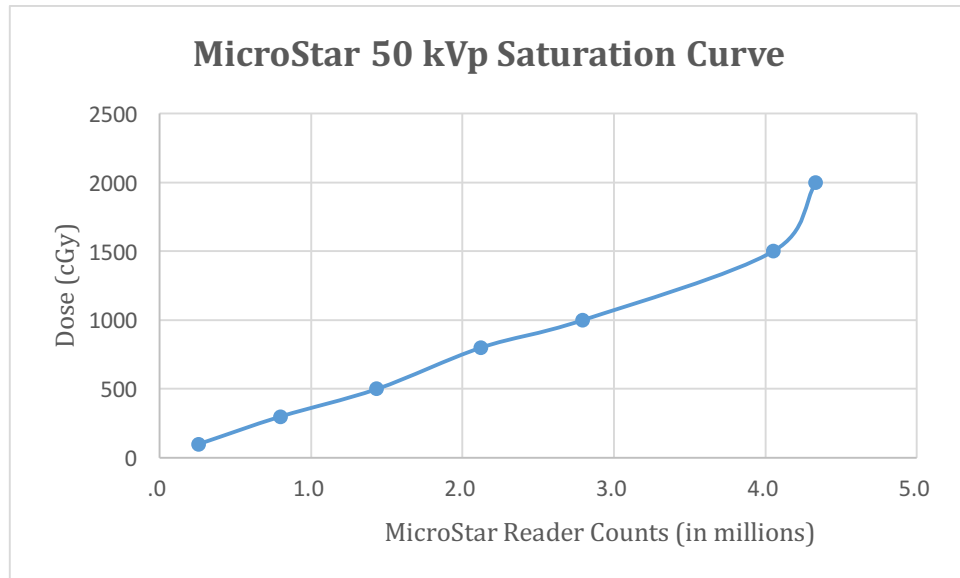


Figure 21: OSLD saturation curve for 50 kVp X-ray measured at 0.5 mm depth with 3.5 cm applicator

OSLD response is the counts per cGy. Table 4 shows the OSLD response ratio of the MV and kV beams. Measurements were taken with both the MV and kV beams at doses of 100, 300, 500, 800, and 1000 cGy in a water medium. These OSLD measurements were read three times each and the average count value was taken. This average count value was divided by the corresponding dosage. The response ratio is between 3.98 and 4.63 and is the average kV response divided by the average MV response at each dosage.

cGy	MV Counts/cGy	kV Counts/cGy	Response Ratio
100	566.12	2622.92	4.63
300	596.07	2694.89	4.52
500	624.13	2929.45	4.69
800	675.4	2688.35	3.98
1000	686.18	2845.71	4.15

Table 4: OSLD response ratio of 50 kVp measurements taken at a depth of 0.5 mm with the 3.5 cm applicator over 6 MV X-rays

Table 5 shows the dose rate and corresponding OSLD response at a depth of 0.5 for each of the applicators. The 2.5 cm applicator at a depth of 0.5 cm has a dose rate of 0.54 Gy/min in water. The 3.0 cm applicator at a depth of 0.5 cm has a dose rate of 0.40 Gy/min in water. The 3.5 cm applicator at a depth of 0.5 cm has a dose rate of 0.48 Gy/min in water. The 4.0 cm applicator at a depth of 0.5 cm has a dose rate of 0.38 Gy/min in water. The 4.5 cm applicator at a depth of 0.5 cm has a dose rate of 0.29 Gy/min in water.

Applicator Diameter (cm)	Dose Rate (Gy/min)	Response (counts/cGy)
2.5	0.54	2916.32
3	0.40	2971.19
3.5	0.48	3001.55
4	0.38	2709.24
4.5	0.29	2700.38

Table 5: OSLD dose rate response

Figures 22 through 26 show response curves for the 2.5, 3.0, 3.5, 4.0, 4.5 cm applicators, respectively. The response curves were created by taking the average of three microStar readings for two OSLD measurements at the depths of 0.5, 1.0, 1.5, 2.0, and 3.0 cm in the water tank for each applicator. The lower the dose the larger the depth of measurement and the higher the energy due to beam hardening through the water medium. These response curves will be used to interpret the OSLDs dependence on accumulated dose and energy. The response curves show a parabolic shape for each applicator.

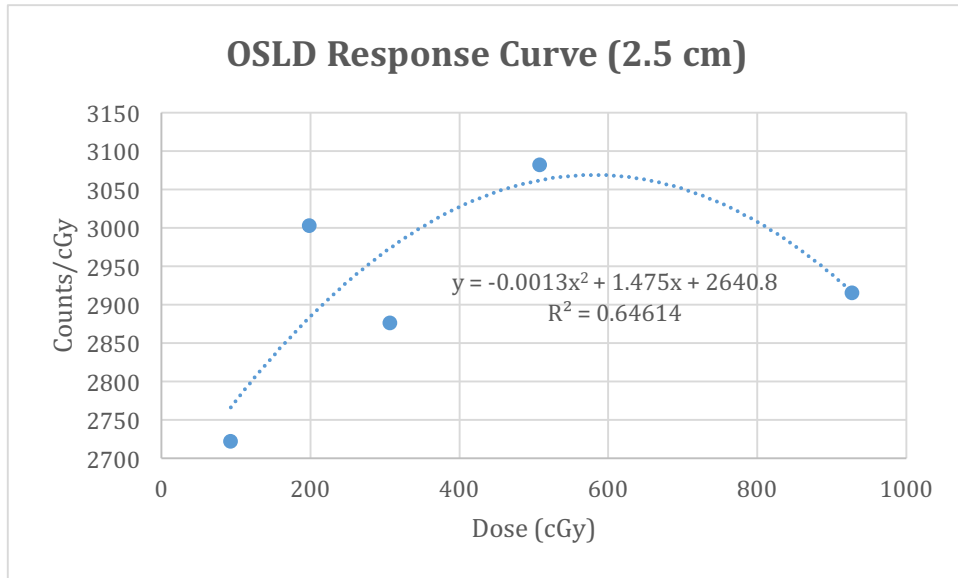


Figure 22: Counts per cGy measured with 2.5 cm applicator at depth of 0.5, 1.0, 1.5, 2.0, and 3.0 mm

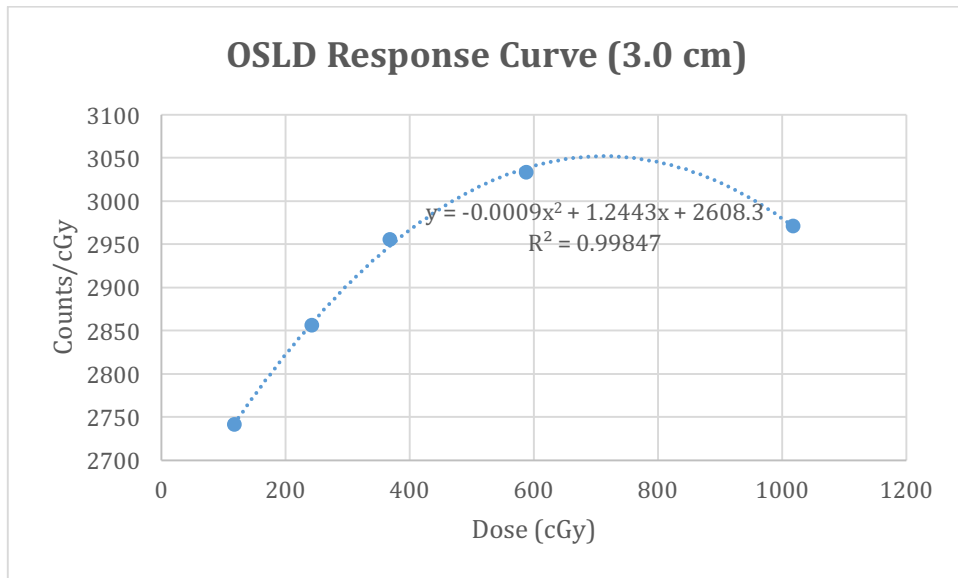


Figure 23: Counts per cGy measured with 3.0 cm applicator at depth of 0.5, 1.0, 1.5, 2.0, and 3.0 mm



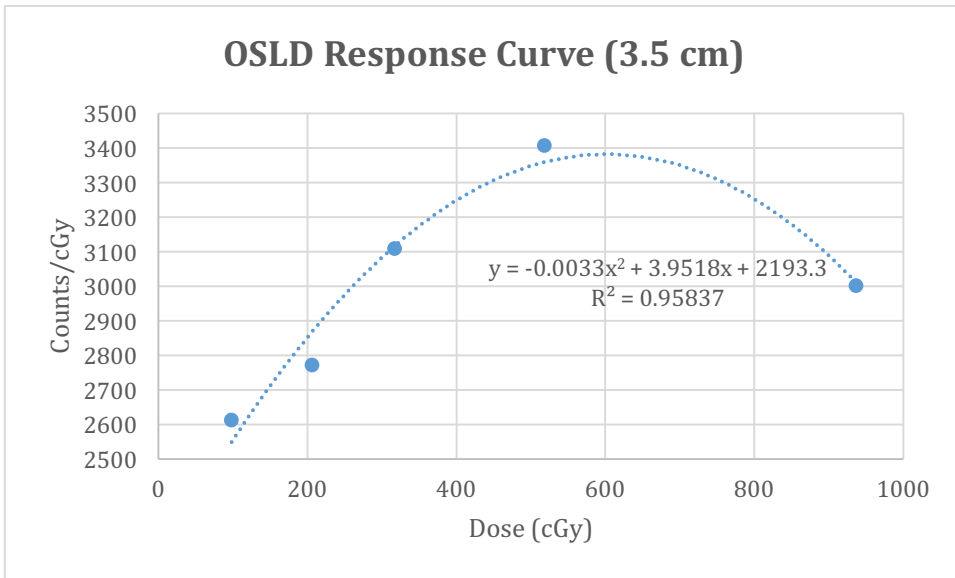


Figure 24: Counts per cGy measured with 3.5 cm applicator at depth of 0.5, 1.0, 1.5, 2.0, and 3.0 mm

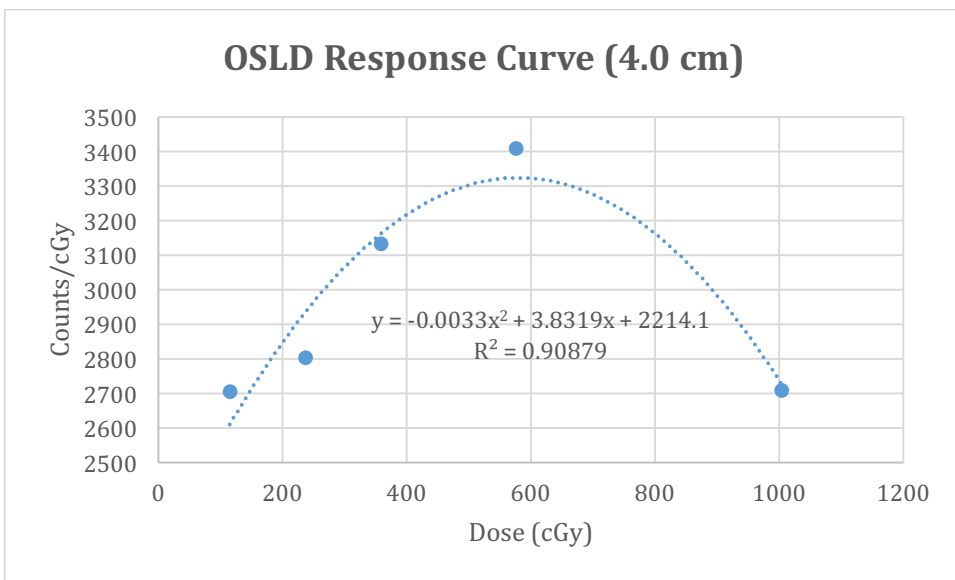


Figure 25: Counts per cGy measured with 4.0 cm applicator at depth of 0.5, 1.0, 1.5, 2.0, and 3.0 mm

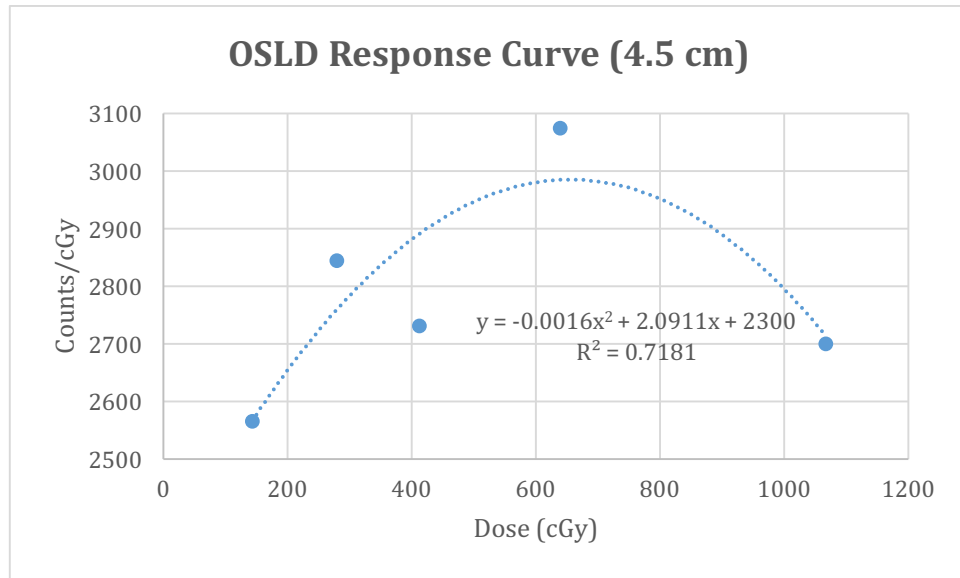


Figure 26: Counts per cGy measured with 4.5 cm applicator at depth of 0.5, 1.0, 1.5, 2.0, and 3.0 mm

Figure 27 is a film calibration curve created using the 3.5 cm applicator. Calibration curves were not created for each applicator because the film is assumed to be energy, accumulated dose, and dose rate independent<sup>15</sup>. This curve was created by taking measurements of 100, 300, 500, 800, 100, 1500, and 2000 cGy at 0.5 mm depth in the water tank. Film does not show a saturation point in this dose range.

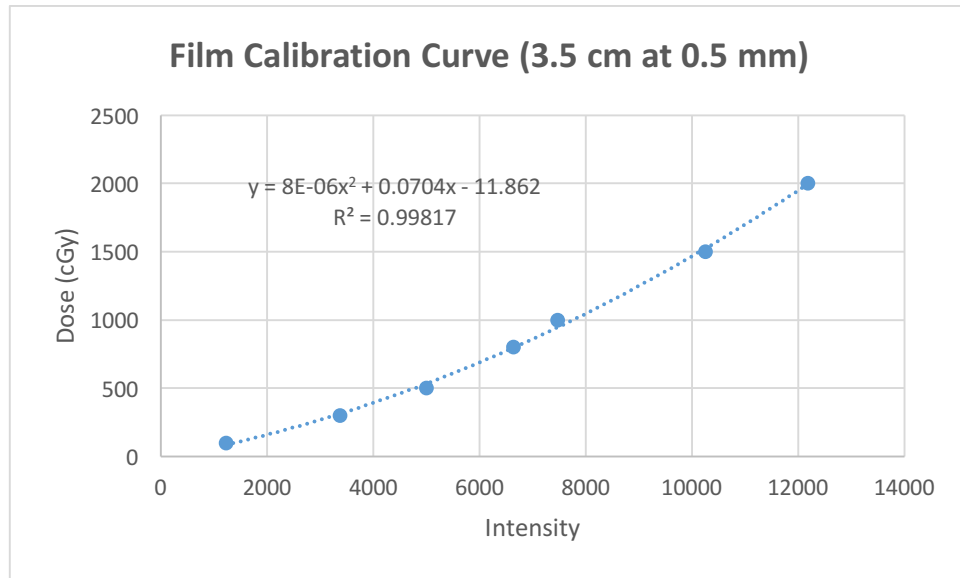


Figure 27: Film calibration curve for the 3.5 cm applicator taken at a depth of 0.5 mm

Table 6 shows the percent difference of the expected and calculated doses from the film measurements for each of the 2.5, 3.0, 3.5, 4.0, and 4.5 cm applicators at the depths of 0.5, 1.0, 1.5, 2.0, and 3.0 cm. The film was scanned with an Epson 10000 XL flatbed scanner. DoseLab software was then used to find the average intensity value of a 2 x 2 mm square around the field center. The dose was then calculated by plugging the average intensity value into the film calibration curve equation. Large percent differences are observed for the 2.5, 3.5, 4.0 and 4.5 cm applicators in the deeper depth lower dose region.

Applicator Diameter (cm)	Depth (cm)	Expected Dose (cGy)	Calculated Dose (cGy)	Percent Difference
2.5	0.5	927	946.48	2.06
2.5	1	508	469.76	8.14
2.5	1.5	307	252.25	21.70
2.5	2	198	143.97	37.53
2.5	3	93	58.82	58.12

3	0.5	1018	989.41	2.89
3	1	588	649.63	9.49
3	1.5	368	405.82	9.32
3	2	242	239.77	0.93
3	3	117	112.69	3.82
3.5	0.5	937	955.20	1.91
3.5	1	519	498.78	4.05
3.5	1.5	317	248.91	27.35
3.5	2	206	197.24	4.44
3.5	3	98	75.72	29.42
4	0.5	1004	1047.43	4.15
4	1	576	549.01	4.92
4	1.5	359	359.58	0.16
4	2	237	206.17	14.96
4	3	115	91.44	25.77
4.5	0.5	1067	1013.40	5.29
4.5	1	639	622.22	2.70
4.5	1.5	412	378.80	8.76
4.5	2	279	219.86	26.90
4.5	3	143	107.68	32.80

Table 6: Percent difference of expected dose and calculated dose for film

Film response is defined as intensity per cGy. Table 7 shows the dose rate and corresponding film response at a depth of 0.5 for each of the applicators. The 2.5 cm applicator at a depth of 0.5 cm has a dose rate of 0.54 Gy/min in water. The 3.0 cm applicator at a depth of 0.5 cm has a dose rate of 0.40 Gy/min in water. The 3.5 cm applicator at a depth of 0.5 cm has a dose rate of 0.48 Gy/min in water. The 4.0 cm applicator at a depth of 0.5 cm has a dose rate of 0.38 Gy/min in water. The 4.5 cm applicator at a depth of 0.5 cm has a dose rate of 0.29 Gy/min in water.

Applicator Diameter (cm)	Dose Rate (Gy/min)	Response (Intensity/cGy)
2.5	0.54	7.98
3	0.40	7.49
3.5	0.48	7.94
4	0.38	7.89
4.5	0.29	7.26

Table 7: Gafchromic film dose rate response

Figures 28 through 32 shows the film response curves for the 2.5, 3.0, 3.5, 4.0, 4.5 cm applicators, respectively. The response curves were created by taking the average of the film intensity value at the depths of 0.5, 1.0, 1.5, 2.0, and 3.0 cm in the water tank for each applicator. The lower the dose the larger the depth of measurement and the higher the energy due to beam hardening through the water medium. These response curves will be used to interpret the Gafchromic film dependence on accumulated dose and energy. The film response curves show a linear relation for each applicator.

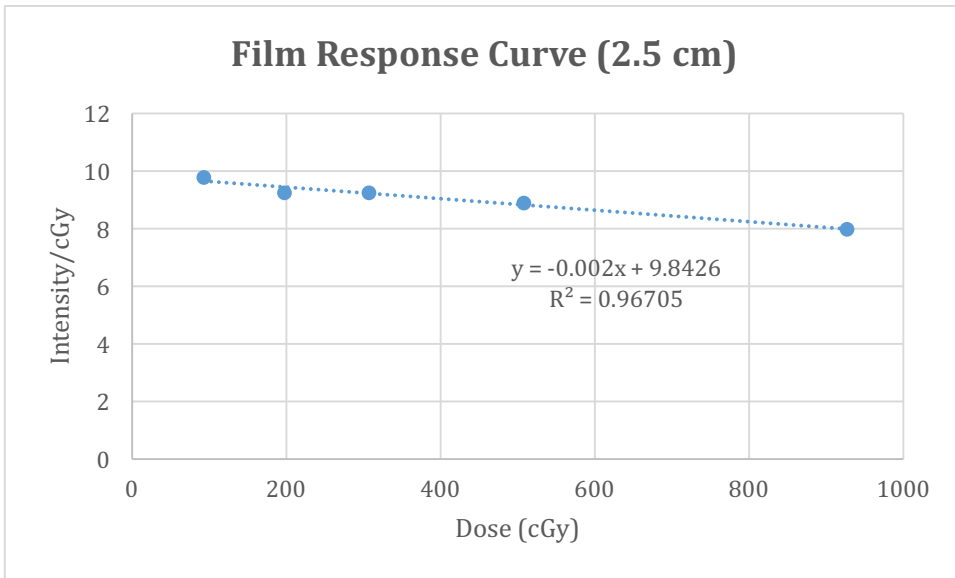


Figure 28: Intensity measured with 2.5 cm applicator at depth of 0.5, 1.0, 1.5, 2.0, and 3.0 mm

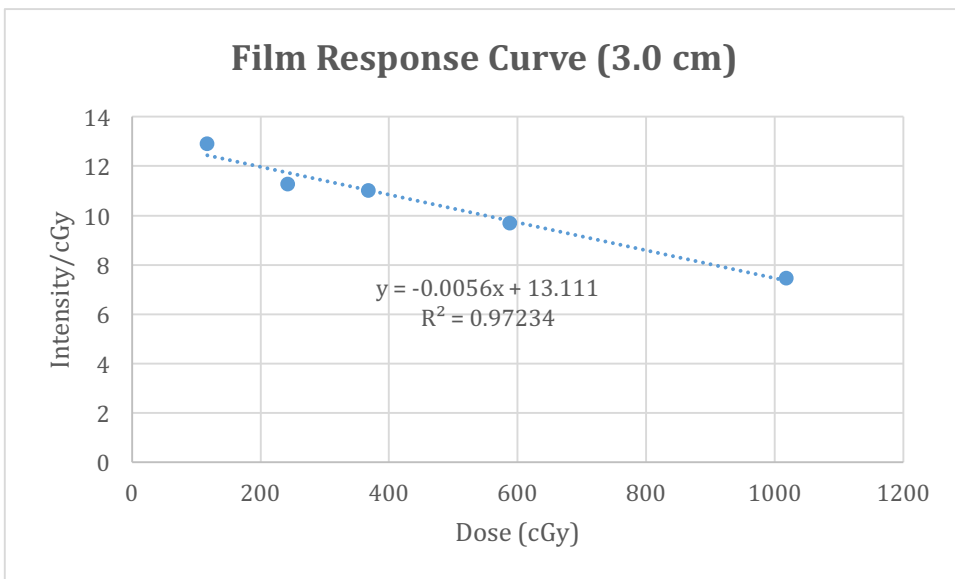


Figure 29: Intensity measured with 3.0 cm applicator at depth of 0.5, 1.0, 1.5, 2.0, and 3.0 mm

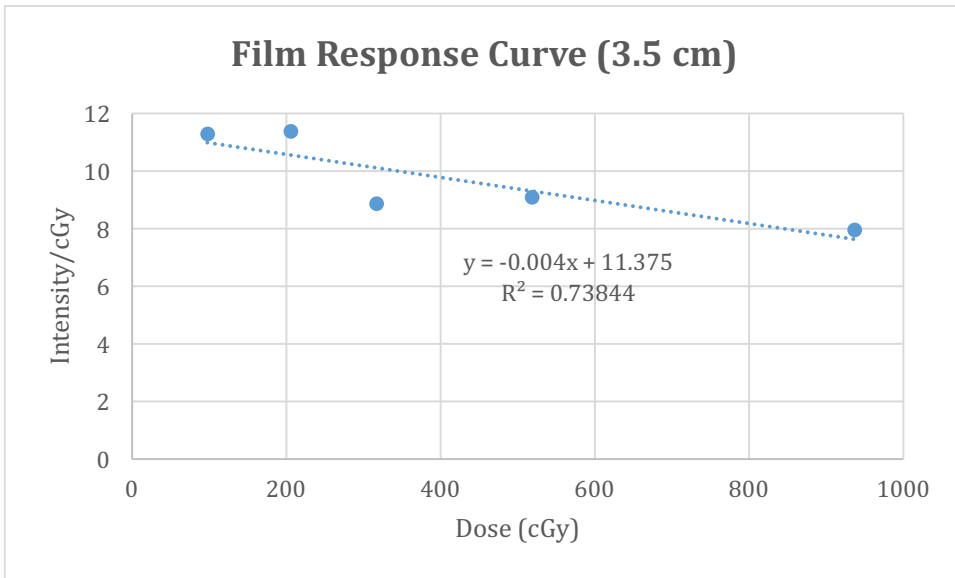


Figure 30: Intensity measured with 3.5 cm applicator at depth of 0.5, 1.0, 1.5, 2.0, and 3.0 mm

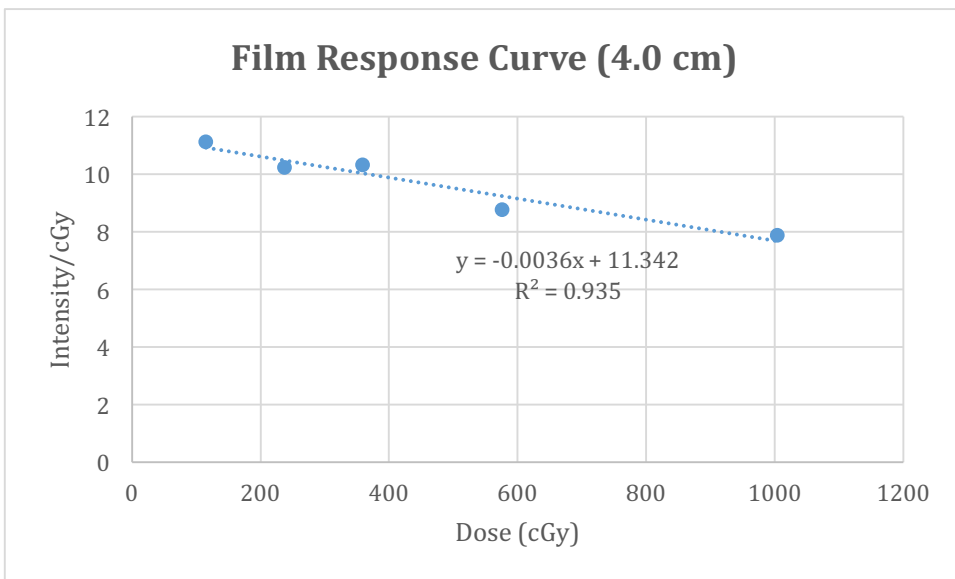


Figure 31: Intensity measured with 4.0 cm applicator at depth of 0.5, 1.0, 1.5, 2.0, and 3.0 mm

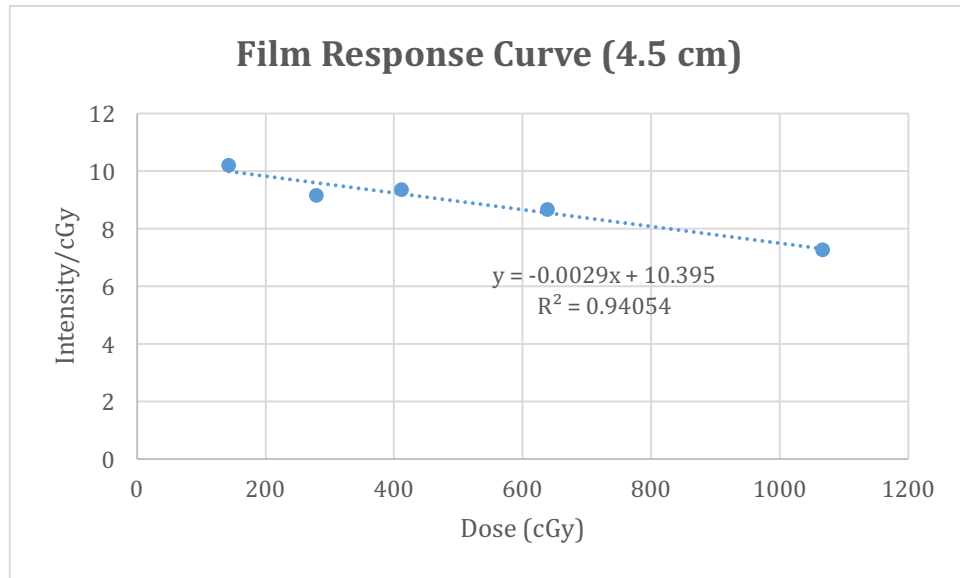


Figure 32: Intensity measured with 4.5 cm applicator at depth of 0.5, 1.0, 1.5, 2.0, and 3.0 mm

## 5. DISCUSSION

The OSLD calibration curves for each applicator shows a good fit with a third order polynomial. This is expected because of the three distinct OSLD sensitivity regions. The first low-dose region is linear due to a constant OSLD sensitivity. The next region is the high-dose quadratic region, where the sensitivity of the OSLD has started to increase. In the last region, the calibration curve starts to become vertical due to signal saturation which is potentially due both to a decrease in OSLD sensitivity and PMT saturation<sup>19</sup>.

The sensitivity of the OSLDs changes with accumulated dose because of the unique electron and hole trap features of the band gap of the  $Al_2O_3:C$  crystal. Electrons trapped in deep traps will only release with heat or UV light, not the LED in the microStar and will not contribute to the dose. In the low-dose linear region, the dosimetric and deep traps compete for electrons. In the high-dose



non-linear region the deep traps have been largely filled and a higher ratio of electrons start to populate the dosimetric trap. This contributes to an increase in signal in the non-linear high-dose region<sup>20</sup>. However, as dose further accumulates the ionization creates an abundance of holes. These holes compete with the dosimetric traps for electrons and reduce the sensitivity<sup>21</sup>. Further, PMT saturation starts to occur in the highest dose region.

Spot checks were performed on each of the calibration curves. This was done to validate the calibration curves and the experimental design. The OSLDs have an inherent uncertainty of 7%. This value is derived using an error propagation analysis from the fact that the OSLDs have an inherent reading error of 5% and kV X-rays show a 5% variation of delivered dose<sup>6,22</sup>. The spot checks showed good agreement with the expected dose when the inherent OSLD uncertainty and the uncertainty of dosimeter placement are taken into account.

It has previously been observed that signal saturation starts above 60 Gy for a 6 MV beam<sup>19</sup>. It is observed from our 50 kVp saturation curve that a decrease in OSLD sensitivity and PMT saturation starts around 15 Gy. This agrees with Jursinic et al. (2009) because the MV to kVp response ratio is between 3.98 and 4.63<sup>19</sup>. It can also be observed that on both the MV and kV saturation curves that the decrease in OSLD sensitivity and PMT saturation starts around 4,000,000 counts.

It is known that the OSLDs exhibit a slight dose rate dependence in the 6 MV to 20 MV energy range<sup>1</sup>. In this range, the OSLDs exhibit a higher response

for a higher dose rate. Table 4 shows that a response fluctuation of about 300 counts/cGy is expected at the same dose rate. This is the same fluctuation in response that was seen in Table 5 with varying dose rates. Therefore, no dose rate dependence was observed for the OSLDs in the 50 kVp dose range.

The OSLD response curves for each applicator shows a parabolic shape. This may seem counter intuitive after the previous discussion of response being linear in the low-dose range followed by quadratic in the high-dose range. This would seem to suggest that as dose accumulates, response should increase up to the point of signal saturation. However, OSLD responses are very energy dependent in the energy ranges where our measurements were collected. The effective energy at the surface of the applicator is 19.5 keV. Due to the spectral shift, the effective energy at 0.5 cm is 27.3 keV, at 1.5 cm it is 31.5 keV, and at 3.0 cm it is 34.0 keV<sup>5</sup>. Further, it is known that Al<sub>2</sub>O<sub>3</sub>:C exhibits maximum response at the photon energy of about 33 KeV<sup>23</sup>. Therefore, the lower the accumulated dose in our experimental design the larger the response to energy. This means that the middle accumulated dose data point's response is increased due to both the energy dependence and the quadratic sensitivity. Whereas, the low accumulated dose region's response is only increased by energy dependence, and the high accumulated dose region's response is only increased due to the quadratic OSLD sensitivity.

The films experiment was designed differently than the OSLD experiment. It was previously known that calibration curves must be built for each applicator for the OSLDs. However, it was unknown if the film would

exhibit dose rate, dose accumulation, and energy independence at the 50 kVp energy. Therefore, this was tested by using a single applicator to build a calibration curve for all of the applicators. This calibration curve was constructed to a higher dosage than the OSLD calibration curves to look for film saturation.

The film showed no sign of saturation up to 20 Gy as seen in figure 27. This is important because the IORT procedure these calibration curves are constructed to deliver 20 Gy. However, the percent difference of the dosage calculated from the calibration curve and the known dosage output by the INTRABEAM at many of the lower accumulated dose points for each of the applicators were beyond clinically acceptable values. Table 7 shows the film did not show any significant dose rate dependence.

The film response curves show a linear trend. This indicates that the response is potentially dependent on energy and dose accumulation. The response (intensity/cGy) at the lowest accumulated dose varies from about 10 to 13 across the applicators. This accounts for the larger percent difference seen for the lower accumulated doses. However, at the highest accumulated dose, the response (intensity/cGy) is about 8 for all of the applicators. This is in agreement with Guerda Massilon et al. that found the response of the film to converge across different energies as the dose accumulates<sup>24</sup>. However, where they found the dose to converge around 100 cGy, this experiment shows the convergence between about 300 and 400 cGy.

## 5.1. CLINICAL IMPLICATIONS

Skin doses between 5 and 15 Gy can lead to moist desquamation, prolonged erythema, permanent epilation, and dermal atrophy in the long term<sup>25</sup>. For skin doses above 15 Gy, edema and acute ulceration may appear as a prompt reaction, epilation and moist desquamation can occur in the short term<sup>25</sup>. The medium and long term reactions potentially include ulceration, dermal atrophy, and dermal necrosis<sup>25</sup>. BCS procedures that utilize the INTRABEAM device are limited to resected tumors that are at least 5 mm from the skin to reduce radionecrosis<sup>26</sup>. At this distance, the skin still receives a relatively high dose of about 10 Gy depending on the applicator. If the applicator is placed any closer than this, the dose to the skin quickly increases up to 20 Gy. Therefore, accurate dosimetry is extremely important for measuring and tracking patient skin dose. This could potentially allow for prophylactic treatments to minimize undesirable outcomes. Currently, there is not a fully understood or well documented approach to meet the unique low energy *in vivo* skin dosimetry requirements for the INTRABEAM device for post BCS treatments. Therefore, understanding the response dependence of OSLDs and Gafchromic EBT 3 film in the low energy, high dose range is important in building reliable calibration curves to perform accurate dosimetry.

## 6. CONCLUSION

The agreement between the spot checks calculated dose and the expected dose indicated that OSLDs are a good option for *in-vivo* INTRABEAM dosimetry. However, the OSLDs are limited to about 10 Gy of accumulated dose due to decreased OSLD sensitivity and PMT saturation. Further research could take more data points and find a more exact point of signal situation and could possibly extend the calibration curves into higher dose ranges. However, the upper limit is around 15 Gy due to signal saturation.

The OSLD response curves were built from the calibration data. This data delivered a dose of 20 Gy to the surface of the applicator and therefore the dose decreased as measurements were taken at deeper depths. This data showed no significant OSLD dependence on dose rate. However, this allowed only for a preliminary investigation into the parabolic shaped response curves that showed both a dependence on dose accumulation and energy. Additional research into the energy dependence of the OSLD response could be performed by delivering the same dose at different depths. For example, if 1, 5 and 10 Gy were delivered at each of the 0.5, 1.0, 1.5, 2.0, and 3.0 cm depths a more rigorous study of the energy dependence of the OSLDs could be performed.

Another possible direction of research would be an investigation of the different sensitivity regions of the OSLDs in the superficial energy range. The current understanding of the different regions of sensitivity is largely derived from MV energy experiments. At these energies the low-dose linear region is below 300 cGy, the high-dose quadratic region is from 300 to 1300 cGy, followed by a region where chip sensitivity changes in an unpredictable way

until signal saturation is reached. This does not reflect what is observed for superficial energies. First, this experiment has shown the over response of the OSLDs in this energy range. This potentially means that the regions of OSLD sensitivity end at a much lower accumulated doses. Second, the MV energy ranges primary interaction is the Compton effect, whereas in the low kV range it is the Photoelectric effect. This could create different sensitivity region trends.

This type of investigation could be achieved by taking a series of low to high accumulated doses with small increments at constant depths normalizing for energy dependence. For example, if doses of increments of 10 cGy were taken at a constant depth from 10 cGy to 1500 cGy the change in OSLD sensitivity could be further evaluated by looking at the calibration and response curves. This could serve as a check to see if OSLD sensitivity has similar regions when the primary reaction changes from the Compton effect to the Photoelectric effect. Further, with the small increments the regions of different sensitivity could be defined better for the low kV range.

Films response has largely not been researched at the low effective energy range created with the INTRABEAM device. This experiment shows potential for it to be used in the clinically desirable dose range up to 20 Gy where the OSLDs cannot be used. The film did not show a dependence on dose rate. However, our calibration curve showed large percent differences for accumulated doses less than about 400 cGy for four out of the five applicators. This seems to indicate a potential energy dependence and inaccuracy in the low dose region.

Further research could be done by creating calibration curves for each of the applicators. Then spot checks could be performed to see if the percent differences are clinically acceptable. These spot checks could serve as a preliminary investigation into accumulated dose dependence. Another potential avenue of investigation is building calibration curves based on different scanner color channels, particularly the red channel, or increasing the dpi. In addition, the energy dependence could be tested by delivering the same dose to different depths in the same manner described above for OSLDs.

#### REFERENCES

1. Nicole T. Ranger (2012). Landauer microStar Reader Quality Assurance Program
2. Carl Zeiss: Offering treatment versatility for multiple tumor types
3. Carl Zeiss. INTRABEAM System from ZEISS: Targeted Radiotherapy
4. Carl Zeiss. INTRABEAM Dosimetry
5. Susha Pillai (2017). Treatment Time Calculations XRS 507185 OHSU. Internal document Oregon Health and Science University radiation oncology department. Contact info pillai@ohsu.edu
6. Ebert, M. A., Asad, A. H. and Siddiqui, S. A. (2009). Suitability of radiochromic films for dosimetry of low energy X-rays. *Journal of Applied Clinical Medical Physics*, 10: 232–240
7. Qi Liu, Frank Schneider, Lin Ma, Frederik Wenz, Carsten Herskind, (2013) Relative Biologic Effectiveness (RBE) of 50 kV X-rays Measured in a

- Phantom for Intraoperative Tumor-Bed Irradiation, International Journal of Radiation Oncology\*Biography\*Physics, Volume 85, Issue 4, Pages 1127-1133,
8. Vaidya JS, Wenz F, Bulsara M, Tobias JS, Joseph DJ, Keshtgar M, Flyger HL, Massarut S, Alvarado M, Saunders C, Eiermann W, Metaxas M, Sperk E, Sütterlin M, Brown D, Esserman L, Roncadin M, Thompson A, Dewar JA, Holtveg HM, Pigorsch S, Falzon M, Harris E, Matthews A, Brew-Graves C, Potyka I, Corica T, Williams NR, Baum M. on behalf of the TARGIT trialists' group (2014). Risk-adapted targeted intraoperative radiotherapy versus whole-breast radiotherapy for breast cancer: 5-year results for local control and overall survival from the TARGIT-A randomised trial. *Lancet*. 2014;383(9917):603–613. Erratum in: *Lancet*, 383(9917):602.
  9. Kraus-Tiefenbacher U, Bauer L, Sceda A et al. Long-term toxicity of an intraoperative radiotherapy boost using low-energy X-rays during breast-conserving surgery. *Int J Radiat Oncol Biol Phys* 2006; 66(2): 377-381
  10. Jursinic, P. A. (2007). Characterization of optically stimulated luminescent dosimeters, OSLDs, for clinical dosimetric measurements. *Med. Phys.*, 34: 4594–4604.
  11. J. R. Kerns. Characterization of Optically Stimulated Luminescent Detectors in Photon & Proton Beams for Use in Anthropomorphic Phantoms. PhD at Texas Medical Center. 2010.
  12. L. Boetter-Jensen, S.W.S. McKeever, A.G. Wintle (2003). *Optically Stimulated Luminescence Dosimetry*



13. Hamamtsu Photonics K.K. (2007). Photomultiplier Tubes Basics and Applications
14. Borca, V. C., Pasquino, M., Russo, G., Grosso, P., Cante, D., Sciacero, P., Girelli, G., Porta, M. R. L. and Tofani, S. (2013), Dosimetric characterization and use of GAFCHROMIC EBT3 film for IMRT dose verification. *Journal of Applied Clinical Medical Physics*, 14: 158–171.
15. Gafchromic™ Dosimetry Media, type EBT-3. White Paper provided by Ashland. [http://www.gafchromic.com/documents/EBT3\\_Specifications.pdf](http://www.gafchromic.com/documents/EBT3_Specifications.pdf)
16. Mobius Medical Systems. DoseLab Pro Manual
17. Chiu-Tsao, S.-T., Ho, Y., Shankar, R., Wang, L. and Harrison, L. B. (2005), Energy dependence of response of new high sensitivity radiochromic films for megavoltage and kilovoltage radiation energies. *Med. Phys.*, 32: 3350–3354
18. Susha Pillai M.S., Richard Crilly Ph.D, Wolfram Laub Ph.D. Commissioning of OSLDs as an *in vivo* Dosimeter in INTRABEAM Radiotherapy for Early Stage Breast Cancer. AAPM presentation.
19. Jursinic P A (2009) Changes in optically stimulated luminescent dosimeter (OSLD) dosimetric characteristics with accumulated dose *Med. Phys.* 37: 132–40
20. Akselrod M S, Bøtter Jensen L and McKeever S W S (2006) Optically stimulated luminescence and its use in medical dosimetry *Radiat. Meas.* 41: S78–99

21. Yukihiro, E. G.; Gaza, R.; McKeever, S. W. S.; Soares, C. G (2004). Optically stimulated luminescence and thermoluminescence efficiencies for high-energy heavy charged particle irradiation in Al<sub>2</sub>O<sub>3</sub>:C. *Radiat. Meas.*, n. 38, p. 59-70.
22. Reft, C. S. (2009), The energy dependence and dose response of a commercial optically stimulated luminescent detector for kilovoltage photon, megavoltage photon, and electron, proton, and carbon beams. *Med. Phys.*, 36: 1690–1699.
23. Kumar, M., Kulkarni, M.S., & Ratna, P. Bhatt, B.C., & Kulkarni, M.S. (Eds.). (2014). *Studies on  $\alpha$ -Al<sub>2</sub>O<sub>3</sub>:C based OSL badge for eye lens monitoring applications in India*. India: Bhabha Atomic Research Centre.17.
24. G. Massillon-JL, S. Chiu-Tsao, I. Domingo-Munoz and M. Chan, "Energy Dependence of the New Gafchromic EBT3 Film:Dose Response Curves for 50 KV, 6 and 15 MV X-Ray Beams," *International Journal of Medical Physics, Clinical Engineering and Radiation Oncology*, Vol. 1 No. 2, 2012, pp. 60-65
25. Balter S, Hopewell JW, Miller DL, Wagner LK, Zelefsky MJ. Fluoroscopically guided interventional procedures: a review of radiation effects on patients' skin and hair. *Radiology*. 2010;254(2):326–41.
26. Williams, Norman R., Katharine H. Pigott, Chris Brew-Graves, & Mohammed R. S. Keshtgar. "Intraoperative radiotherapy for breast cancer." *Gland Surgery* [Online], 3.2 (2014): 109-119. Web. 1 Jul. 2017

